

Measurement of Body-Centered Cubic Gold and Melting under Shock CompressionR. Briggs,^{1,*} F. Coppari,¹ M. G. Gorman,¹ R. F. Smith,¹ S. J. Tracy,² A. L. Coleman,¹ A. Fernandez-Pañella,¹ M. Millot,¹ J. H. Eggert,¹ and D. E. Fratanduono¹¹*Lawrence Livermore National Laboratory, Livermore, California 94500, USA*²*Geophysical Laboratory, Carnegie Institution of Washington, Washington, D.C. 20015, USA*

(Received 21 March 2019; published 24 July 2019)

We combined laser shock compression with *in situ* x-ray diffraction to probe the crystallographic state of gold (Au) on its principal shock Hugoniot. Au has long been recognized as an important calibration standard in diamond anvil cell experiments due to the stability of its face-centered cubic (fcc) structure to extremely high pressures ($P > 600$ GPa at 300 K). This is in contrast to density functional theory and first principles calculations of the high-pressure phases of Au that predict a variety of fcc-like structures with different stacking arrangements at intermediate pressures. In this Letter, we probe high-pressure and high-temperature conditions on the shock Hugoniot and observe fcc Au at 169 GPa and the first evidence of body-centered cubic (bcc) Au at 223 GPa. Upon further compression, the bcc phase is observed in coexistence with liquid scattering as the Hugoniot crosses the Au melt curve before 322 GPa. The results suggest a triple point on the Au phase diagram that lies very close to the principal shock Hugoniot near ~ 220 GPa.

DOI: [10.1103/PhysRevLett.123.045701](https://doi.org/10.1103/PhysRevLett.123.045701)

Gold (Au) is perhaps the most recognizable and precious of the noble metals. It is one of the least reactive chemical elements and the face-centered cubic (fcc) crystal structure is predicted to be stable over hundreds of GPa [1–5]. Its chemical inertness and the stability of its crystal structure, along with its scattering efficiency, makes Au a particularly useful pressure standard for high-pressure diamond anvil cell (DAC) experiments [6,7]. Shock compression experiments up to 10 TPa (1 TPa = 1000 GPa = 10 MBar) showed no obvious discontinuities in shock velocity or particle velocity data, which has been used to suggest the absence of solid-solid phase transitions and a very small volume change on melting [8–13].

A wide range of *ab initio* calculations first predicted structural transformations in Au at pressures ranging between 151 and 620 GPa from the fcc crystal structure (with *ABC* stacking) to a variety of close-packed structures with alternate stacking of the Au atoms in the close packed direction: double hexagonal close packed (dhcp) with *ABAC* stacking [1,2], hexagonal close packed (hcp) with *AB* stacking [1–5], and also an *ABCACB* stacking structure [2]. In 2002, a body centered cubic (bcc) structure was proposed to be a stable at high pressure, due to hybridization of the *5p* states with the *5d* band [4]. More recently, first principles calculations predicted a transformation to the hcp and bcc structures at 255 and 480 GPa, respectively, along the 300 K isotherm [14].

The theoretical prediction for phase transition along the 300 K isotherm were in good agreement with conventional DAC data that used *in situ* heating with x-ray diffraction to observe the appearance of new Bragg peaks that could be

indexed to a hcp structure, at ~ 248 GPa and 860 K [1]. Upon cooling slowly to room temperature, those new peaks increased in intensity as the fcc peaks decreased. Recent double-stage DAC and toroidal DAC 300 K isotherm measurements show only the fcc structure at all pressures up to 1065 and 603 GPa, respectively [7,15]. Due to these discrepancies between different static measurements and theoretical predictions, our current understanding of the Au phase diagram is inadequate and further experimental data are needed to benchmark first principles calculations. Shock compression provides an alternative pathway to probing materials at high pressures and temperatures beyond the reach of static compression in the DAC. Recent advances in user facilities, such as the Dynamic Compression Sector (DCS) at the Advanced Photon Source (APS) synchrotron, have allowed high-quality synchrotron x-ray diffraction (XRD) to be collected under shock compression [16].

In this Letter, we present our study of the crystal structures of Au up to a maximum pressure of 322(27) GPa along the principal shock Hugoniot. The fcc phase is observed up to 169(8) GPa. Coexistence of fcc with bcc Au is observed at 223(11) and 253(19) GPa. The fcc to bcc phase transition is completed by 262(10) GPa, where we observe a coexistence of bcc Au with liquid scattering on the Hugoniot, suggesting only a small pressure range on the shock Hugoniot where the bcc phase alone is stable. At the maximum pressure obtained, 322(27) GPa, only liquid Au is observed and melting on the Hugoniot is complete. The results indicate the presence of a triple point near the principle shock Hugoniot at $\sim 220(20)$ GPa. These measurements improve

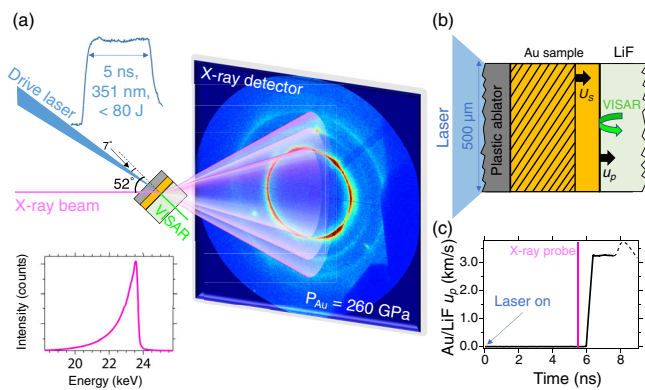


FIG. 1. (a) Schematic overview of experimental setup at the dynamic compression sector, APS. The x-ray beam (spectral flux shown) probes the sample at an angle of 52° from the sample normal, with the diffracted x rays from the sample recorded on the detector ~ 100 mm away. (b) Sketch of the target assembly. The x-ray beam probes the full sample at a time equal to or before the shockwave (traveling at shock velocity U_s) reaches the LiF window. The compressed region behind the shock front is highlighted by the shaded region in the Au sample. (c) The measured Au/LiF particle velocity history (u_p) from VISAR for the compressed data are also shown; the dashed portion of the VISAR trace is related to the reverberation or release wave interactions that occur several nanoseconds after the sample probe time.

our understanding of the Au phase diagram and bolster the recent theoretical predictions [14].

Experiments were carried out at DCS [16], using the geometry shown in Fig. 1(a). A high-energy laser (351 nm) [17], focused to a $500 \mu\text{m}$ diameter focal spot, sent an ablatively driven shockwave through the sample package. As shown in Fig. 1(b), shock targets consisted of $50 \mu\text{m}$ polyimide with an Al flash coating ($\sim 0.1 \mu\text{m}$) on one side and a deposition of a $6.8 \mu\text{m}$ thick Au layer on the other. A $500 \mu\text{m}$ thick single crystal [100] Lithium Fluoride (LiF) window was glued to the polyimide/Au with an estimated glue thickness of $1\text{--}3 \mu\text{m}$. The LiF was coated with $\sim 0.1 \mu\text{m}$ of Al to enhance reflectivity for velocity measurements. Further information can be found in the Supplemental Material [18].

The drive laser and x rays were 7° and 52° from sample normal, respectively [Fig. 1(a)]. Laser energies of up to ~ 75 J (using a 10 ns flat top pulse shape) and ~ 63 J (using a 5 ns flat top pulse shape) sent shocks of up to ~ 322 GPa through the Au. The distinct pressure states that could be accessed were dependent on the discrete laser intensities available. Pressure was determined using a point VISAR (velocity interferometer system for any reflector) and from impedance matching of the Au sample and LiF window [18].

X-ray diffraction measurements were collected on a Rayonix SX165 flat panel CCD detector. A single x-ray pulse of ~ 100 ps duration was isolated from the APS Hybrid filling mode using a high-speed chopper system. The x rays were timed to probe the Au sample just before

shock entry into the LiF window, so as to avoid late time pressure release states. A pink x-ray beam from a U17 undulator, shown inset to Fig. 1(a), provided a quasi monochromatic x-ray flux spectrum with a peak energy of 23.54 keV ($\lambda = 0.5266 \text{ \AA}$) [18]. The sample target package was placed in the vacuum chamber in transmission geometry, with the sample to detector distances determined using a polycrystalline silicon x-ray standard [19–21]. Two sample-detector distances of 111.75 mm and 92.96 mm were used during the experiments. Due to the asymmetric spectral flux of the x-ray source [Fig. 1(a)], standard peak fitting functions (Gaussian, Lorentzian, or Pseudo-Voigt etc.) are not suitable to fit the diffraction peaks. Here, we use a convolution of a Gaussian peak with an exponential tail (“Exp-Gauss”) to fit the experimental data [18].

X-ray diffraction (XRD) measurements were collected on the shock Hugoniot up to a maximum pressure of 322(27) GPa. The lowest pressure obtained in this study [$P = 169(8)$ GPa] was obtained using the maximum energy of the laser with a 10 ns laser pulse length (~ 75 J); the remaining data used a 5 ns pulse length. Figure 2 shows a series of integrated XRD profiles from 0 GPa (ambient foil before compression) up to maximum pressure. At 169 GPa, a shift of the ambient fcc peaks to higher Q [where $Q = 4\pi \sin \theta / \lambda$ and λ is defined as the peak of the spectral flux from Fig. 1(a)] is observed as the unit cell is compressed. Least squares fitting of all diffraction peaks, using the “Exp-Gauss” function, shows a good fit to expected positions of ambient fcc Au and compressed fcc Au (purple triangles in Fig. 2). Due to the highly textured nature of the deposited Au sample, intensity variations are observed around the Debye-Scherrer rings. Textured peaks from uncompressed material ahead of the shockwave are highlighted by white ellipses in Fig. 2(b); see Supplemental Material for full x-ray diffraction image of the uncompressed foil [18]. There is a change in texture of the fcc Au as the compressed fcc region becomes more powderlike due to dislocation formation and plastic flow during shock compression [22,23]. The peak positions of fcc Au agree well with the expected shift in d spacing along the principal Hugoniot (purple triangles and solid lines in Fig. 3).

The next pressure state on the Hugoniot was $P = 223(11)$ GPa. Faint peaks were visible that do not fit to the ambient or compressed fcc Au; these new peaks are shown by green triangles in Fig. 2. There is clear texture of the compressed fcc peaks at similar azimuthal angles as the pre-shot ambient fcc Au peaks, and also observed is a much less textured powder ring in close proximity to the fcc (111) peak. The three peaks found at $Q = 3.112 \text{ \AA}^{-1}$, 4.391 \AA^{-1} , and 5.361 \AA^{-1} (d -spacing values of 2.019 \AA , 1.431 \AA , and 1.172 \AA) can be indexed to a body centered cubic structure. At slightly higher pressure, $P = 253(19)$ GPa, both compressed fcc Au and bcc Au peaks are observed but the relative intensity of bcc and fcc is

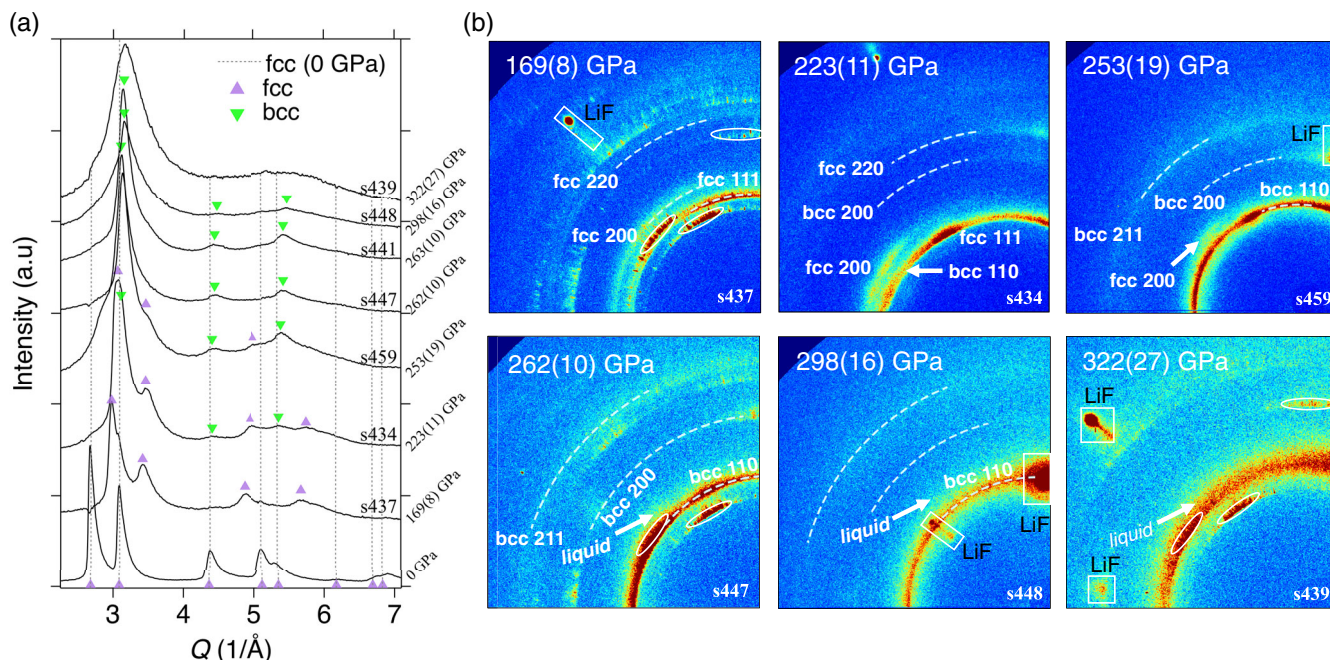


FIG. 2. (a) Radially integrated x-ray diffraction profiles for shock compressed fcc (purple triangles), fcc + bcc (purple and green triangles), bcc (green triangles) + liquid, and liquid only regions along the shock Hugoniot. Ambient fcc peaks were also measured in a preshot exposure and have been subtracted from each compressed profile (the dotted lines represent ambient fcc Au peak locations). The intensity of the liquid only shot at 322 GPa was increased ($\times 2$) to a similar scale as all other data. (b) A selection of the raw x-ray diffraction images with fcc, bcc, or liquid scattering labeled. Strong single crystal Bragg reflections from the LiF window are highlighted by white boxes. Ambient fcc peaks, due to the uncompressed Au ahead of the shockwave, are highlighted by white ellipses. These features are masked in the integrated patterns in Fig. 2(a). All raw data can be found in the Supplemental Material [18].

higher. The positions of the bcc (110), (200), and (211) peaks are plotted in Fig. 3 (green dashed lines) using a previously determined Au Hugoniot P - ρ path to

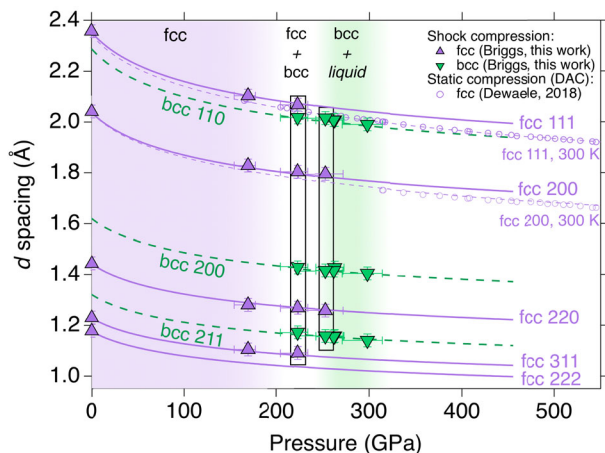


FIG. 3. Lattice d -spacing vs pressure plot for fcc (upward triangles) and bcc (downward triangles) Bragg peaks. The shaded regions represent the fcc, fcc + bcc, and bcc + liquid phases observed in this Letter. The two square boxes represent data collected from the same shot, which are also shown in Fig. 4. Solid purple lines represent the fcc Au, along the Hugoniot (from Ref. [13]), dashed green lines represent bcc Au. The dashed purple line with open symbols represents static DAC measurements of fcc Au that extend beyond 500 GPa [15].

determine the d spacings for all the fcc and bcc reflections over our detectable range [13]. An excellent agreement with the d -spacing values determined from our x-ray diffraction measurements is observed (green triangles).

At 262(10) GPa and above, fcc Au is not observed and instead the bcc Au is observed with a significant increase in diffuse scattering signal indicative of liquid Au; we note that this is not a broadening of the bcc or fcc peaks and is clearly distinct scattering from partially melted Au. At 322(27) GPa, only liquid scattering signal is observed, indicating the shock Hugoniot has left the solid or liquid coexistence along the melting curve. A large coexistence range (~ 116 GPa) of solid Au and liquid Au was predicted by the multiphase EOS by Kerley [24], with melting beginning at 212 GPa and completing at 328 GPa. In this Letter, we observe diffraction patterns with clear solid and liquid diffraction at pressures of 262 and 298 GPa, suggesting a coexistence of at least 36 GPa and no more than ~ 72 GPa (no detectable liquid at 250 GPa and no detectable solid at 322 GPa).

From our x-ray diffraction data, we are able to calculate the density of the phase from the volume of the unit cell. We take an average of the lattice parameter, a , calculated from the d spacing of each observed peak to determine the volume per atom. The density, calculated from x-ray diffraction, is plotted against pressure, determined from velocimetry measurements, in Fig. 4. Our solid Au data

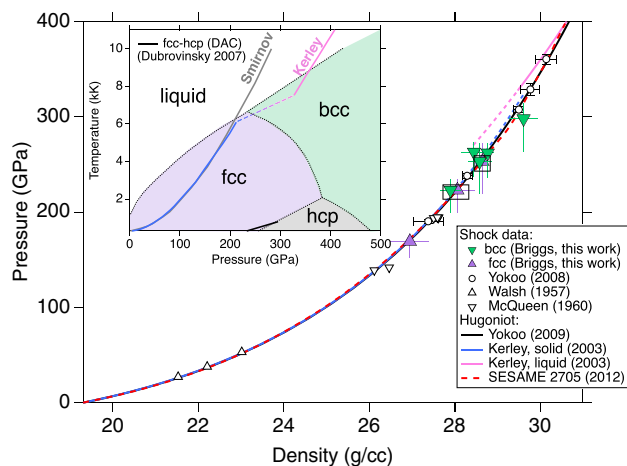


FIG. 4. Pressure vs density for Au. Open symbols represent shock Hugoniot data [8,12,27], with calculated Hugoniot curves plotted as solid lines [13,24,25]. Inset shows the proposed phase diagram of Au based on first principles calculations [14]. Our data (solid triangles) overlay well with the existing Hugoniot curves [13,24,25]. The dashed lines are extrapolations to regions where the Kerley EOS suggests that melting should occur [24].

points agree well, within experimental error, with the Yokoo Hugoniot data (black line and open circles) [13], the Kerley multiphase EOS (blue and pink lines) [24], and the SESAME 2705 EOS (red dashed line) [25]. Whilst there have been recent advancements in characterizing the structure of shock compressed liquids [26], extracting accurate density measurements of the shocked liquid sample from diffraction data alone has not yet been demonstrated.

By using the Rankine-Hugoniot equation, based on conservation of energy, $E = \frac{1}{2}P(\rho - \rho_0/\rho\rho_0)$ [28], where P is the pressure determined from impedance matching, ρ is the density from x-ray diffraction measurements, and ρ_0 is the initial density (19.3 g/cm³), we can compare our measured Hugoniot data with the calculated Hugoniot and melting curve, and provide a useful description of the Au phase diagram in pressure-energy space (Fig. 5). The gradient of the fcc and bcc melting slopes are estimated from the Clapeyron slope of the predicted melting curve, shown inset to Fig. 4 [14], and from the volume change on melting from the shock Hugoniot [13]. The dashed lines in Fig. 5 represent proposed phase boundaries that must encompass the experimental data (within experimental bounds) and are estimated based on the data presented here and used for illustrative purposes only.

Since no measure of temperature is made during these shock experiments, we rely on theoretical calculations to determine the Hugoniot path in P - T space. A recent first principles prediction of the phase diagram of Au, which found bcc Au was a stable phase at high pressure and high temperature, is plotted as an inset to Fig. 4 [14]. The calculated shock Hugoniot are also plotted in P - T space, the blue-to-pink dashed line represents the melt line between the Kerley solid and liquid EOS. All Hugoniot

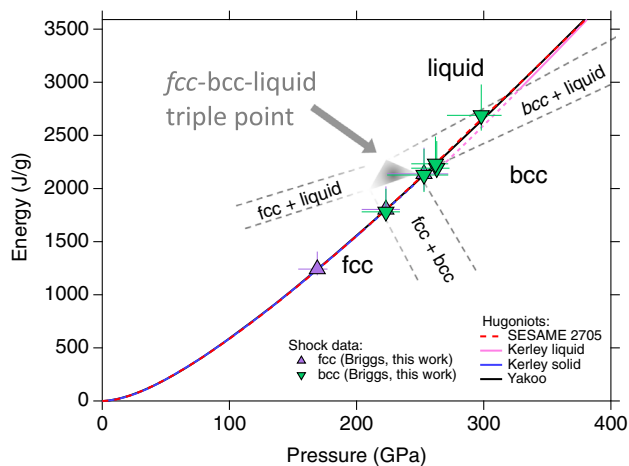


FIG. 5. Energy vs pressure plot for Au. Calculated Hugoniot data are plotted as solid lines, with the blue and pink dashed lines representing the extension of the Kerley solid EOS and liquid EOS, respectively, [24] to the pressures where only solid or solid-liquid data are observed. The dashed black lines are representative phase boundaries in energy-pressure space, with the gray shaded region representing the region of the fcc-bcc-liquid triple point.

are plotted using an initial density of $\rho_0 = 19.3$ g/cm³ and our measured data show good agreement with the principal Hugoniot in P - ρ . We note that the uncertainty in the measurement of the initial foil density could suggest porosity of the starting foils, which would result in higher temperatures along the Hugoniot and shock melting at lower pressures. Based on the uncertainty in the initial density measurement ($\sim 3.6\%$, resulting in $\rho_0 = 18.6$ g/cm³), melting on the porous Hugoniot would begin ~ 50 GPa lower than observed in this Letter due to a sharper increase in temperature [28].

In our experiments, a rapid entropy increase that is generated under shock compression causes a significant increase in temperature, allowing us to probe a small region of the phase diagram predicted by Smirnov [14]. In static compression experiments above 230 GPa, heating of the fcc phase is required to change the crystal structure [1]. These results emphasize the important effect of temperature on the structural stability of Au at a high pressure. The melting curve in the Smirnov predicted phase diagram was estimated using the Lindemann criterion [29] and the phase diagram suggests that Au along the Hugoniot would melt from the fcc phase [14]. In this Letter, we only saw bcc Au in coexistence with the fcc and with the liquid phases. The close vicinity of phase coexistence of fcc-bcc and bcc-liquid suggests a triple point in Au that lies very close to the principle shock Hugoniot at $P \sim 220 \pm 20$ GPa (grey shaded region in Fig. 5). Whilst we cannot determine the temperature of the triple point in this Letter, its pressure is very close to the value predicted from first principle calculations of $P \sim 235$ GPa (in that work the temperature of the triple point was calculated at ~ 6600 K).

In this Letter, we observe the first evidence for bcc Au on the principal shock Hugoniot. The Hugoniot follows the fcc + bcc phase region between 225 and 253 GPa, after which the Hugoniot passes through a small region of bcc-only phase space before very quickly reaching the melt curve. We observe bcc Au in coexistence with the liquid between 262 and 298 GPa, after which only liquid Au is observed. This work highlights the requirement for further first principle calculations, at finite temperatures, to determine a new multiphase EOS of Au that considers the fcc to bcc phase transition we have discovered in this Letter.

We thank Xiaoming Wang, Nicholas Sinclair, Adam Schuman, Paulo Rigg, and the staff of the Dynamic Compression Sector for assistance with laser experiments. We thank Yoshi Toyoda for his assistance with VISAR measurements during the laser experiments. We would like to thank Carol A. Davis for her help in preparing the gold targets. This work was performed under the auspices of the U.S. Department of Energy by Lawrence Livermore National Laboratory under LLNL's Laboratory Directed Research and Development (LDRD) Program under Grants No. 18-ERD-001 and No. 18-ERD-012. Lawrence Livermore National Laboratory is operated by Lawrence Livermore National Security, LLC, for the U.S. Department of Energy, National Nuclear Security Administration under Contract No. DE-AC52-07NA27344. This publication is also based upon work performed at the Dynamic Compression Sector supported by the DOE/NNSA under Award No. DE-NA0002442 and operated by Washington State University. This research used resources of the Advanced Photon Source, a DOE Office of Science User Facility operated for the DOE Office of Science by Argonne National Laboratory under Contract No. DE-AC02-06CH11357.

Note added in the proof.—Recently, further experimental work by S. Sharma *et al.* reported on the phase transition to bcc gold and melting under shock compression (see reference [30]).

*briggs14@llnl.gov

- [1] L. Dubrovinsky, N. Dubrovinskaia, W. A. Crichton, A. S. Mikhaylushkin, S. I. Simak, I. A. Abrikosov, J. S. de Almeida, R. Ahuja, W. Luo, and B. Johansson, *Phys. Rev. Lett.* **98**, 045503 (2007).
- [2] T. Ishikawa, K. Kato, M. Nomura, N. Suzuki, H. Nagara, and K. Shimizu, *Phys. Rev. B* **88**, 214110 (2013).
- [3] R. Ahuja, S. Rekh, and B. Johansson, *Phys. Rev. B* **63**, 212101 (2001).
- [4] P. Söderlind, *Phys. Rev. B* **66**, 176201 (2002).
- [5] J. C. Boettger, *Phys. Rev. B* **67**, 174107 (2003).
- [6] A. Dewaele, P. Loubeyre, and M. Mezouar, *Phys. Rev. B* **70**, 094112 (2004).
- [7] N. Dubrovinskaia, L. Dubrovinsky, N. A. Solopova, A. Abakumov, S. Turner, M. Hanfland, E. Bykova, M. Bykov, C. Prescher, V. B. Prakapenka, S. Petitgirard, I. Chuvashova,

- B. Gasharova, Y. L. Mathis, P. Ershov, I. Snigireva, and A. Snigirev, *Sci. Adv.* **2**, e1600341 (2016).
- [8] J. M. Walsh, M. H. Rice, R. G. McQueen, and F. L. Yarger, *Phys. Rev.* **108**, 196 (1957).
- [9] L. V. Al'tshuler, K. K. Krupnikov, and M. I. Brazhnik, *Sov. Phys. JETP* **34**, 614 (1958).
- [10] A. H. Jones, W. M. Isbell, and C. J. Maiden, *J. Appl. Phys.* **37**, 3493 (1966).
- [11] L. V. Al'tshuler, A. A. Bakanova, I. P. Dudoladov, E. A. Dynin, R. F. Trunin, and B. S. Chekin, *J. Appl. Mech. Tech. Phys.* **22**, 145 (1981).
- [12] R. G. McQueen and S. P. Marsh, *J. Appl. Phys.* **31**, 1253 (1960).
- [13] M. Yokoo, N. Kawai, K. G. Nakamura, K. I. Kondo, Y. Tange, and T. Tsuchiya, *Phys. Rev. B* **80**, 104114 (2009).
- [14] N. A. Smirnov, *J. Phys. Condens. Matter* **29**, 105402 (2017).
- [15] A. Dewaele, P. Loubeyre, F. Occelli, O. Marie, and M. Mezouar, *Nat. Commun.* **9**, 2913 (2018).
- [16] X. Wang, P. Rigg, J. Sethian, N. Sinclair, N. Weir, B. Williams, J. Zhang, J. Hawreliak, Y. Toyoda, Y. Gupta, Y. Li, D. Broege, J. Bromage, R. Earley, D. Guy, and J. Zuegel, *Rev. Sci. Instrum.* **90**, 053901 (2019).
- [17] D. Broege, S. Fochs, G. Brent, J. Bromage, C. Dorrer, R. F. Earley, M. J. Guardalben, J. A. Marozas, R. G. Roides, J. Sethian, X. Wang, D. Weiner, J. Zweiback, and J. D. Zuegel, *Rev. Sci. Instrum.* **90**, 053001 (2019).
- [18] See Supplemental Material at <http://link.aps.org/supplemental/10.1103/PhysRevLett.123.045701> for a table of experimental results, raw x-ray diffraction profiles, velocimetry results, and a description of x-ray diffraction analysis.
- [19] A. P. Hammersley, S. O. Svensson, M. Hanfland, A. N. Fitch, and D. Hausermann, *High Press. Res.* **14**, 235 (1996).
- [20] C. Prescher and V. B. Prakapenka, *High Press. Res.* **35**, 223 (2015).
- [21] T. Sun and K. Fezzaa, *J. Synchrotron Radiat.* **23**, 1046 (2016).
- [22] C. E. Wehrenberg, D. McGonegle, C. Bolme, A. Higginbotham, A. Lazicki, H. J. Lee, B. Nagler, H. S. Park, B. A. Remington, R. E. Rudd, M. Sliwa, M. Suggit, D. Swift, F. Tavella, L. Zepeda-Ruiz, and J. S. Wark, *Nature (London)* **550**, 496 (2017).
- [23] R. Briggs *et al.*, *Phys. Rev. Lett.* **118**, 025501 (2017).
- [24] G. I. Kerley, Sandia National Laboratories report, No. SAND2003-3784, 2003.
- [25] J. C. Boettger, K. G. Honnell, J. H. Peterson, C. W. Greeff, and S. D. Crockett, *AIP Conf. Proc.* **1426**, 812 (2012).
- [26] M. G. Gorman, A. L. Coleman, R. Briggs, R. S. McWilliams, D. McGonegle, C. A. Bolme, A. E. Gleason, E. Galtier, H. J. Lee, E. Granados, M. Sliwa, C. Sanloup, S. Rothman, D. E. Fratanduono, R. F. Smith, G. W. Collins, J. H. Eggert, J. S. Wark, and M. I. McMahon, *Sci. Rep.* **8**, 16927 (2018).
- [27] M. Yokoo, N. Kawai, K. G. Nakamura, and K. I. Kondo, *Appl. Phys. Lett.* **92**, 051901 (2008).
- [28] Y. B. Zel'dovich and Y. P. Raizer, *Physics of Shock Waves and High-Temperature Hydrodynamic Phenomena* (Dover Publications, Mineola, 2002).
- [29] F. A. Lindemann, *Phys. Z.* **11**, 609 (1910).
- [30] S. M. Sharma *et al.*, following Letter, *Phys. Rev. Lett.* **123**, 045702 (2019).